# Dispersion of Particle Pulses in Fluidized Beds Measured by Positron Emission Tomography

**C. Dechsiri and E. A. Van der Zwan**
Dept. of Chemical Engineering, University of Groningen, 9747AG Groningen, The Netherlands

**H. G. Dehling**
Dept. of Mathematics, University of Bochum, Bochum 44780, Germany

**Alex. C. Hoffmann**
Dept. of Physics, University of Bergen, Allégaten 55, 5007 Bergen, Norway

*DOI 10.1002/aic.10347*
*Published online in Wiley InterScience (www.interscience.wiley.com).*

*The dispersion of pulses of a range of shapes through a bubbling fluidized bed has been studied using an ECAT EXACT HR+ PET camera. The equipment and materials used made it possible to label actual bed particles with a radioactive labeler for use as tracer. The experimental equipment and procedure as well as the data analysis procedure are described. The results are shown as bitmaps, 3-D plots, and contour plots of the relative tracer concentration during 1-s time intervals. The particle pulse is shown to exhibit a cyclical axial motion while it is being dispersed. The results are compared with a phenomenological stochastic model for particle dynamics. It is further shown that the model, which is based on the notions of upward material transport with the fluidization bubbles and material descent with dispersion in the bulk, qualitatively captures all the essential features. Material transport only in bubble wakes, however, could not account quantitatively for the results. The discrepancy is likely attributable to "gulf streaming" in the bed, a phenomenon that should be studied experimentally and accounted for in models for particle dynamics in fluidized beds.* © 2005 American Institute of Chemical Engineers
*AIChE J,* 51: 791–801, 2005
*Keywords: fluidization, positron emission tomography, dispersion, pulse, gulf streaming*

## Introduction

Recently the method of "positron emission particle tracking" (PEPT) was introduced to study particle dynamics in process apparatus. Much of the early work was done at the University of Birmingham,[1] including work on fluidized beds (for example, Stein et al.[2,4] and Snieders et al.[3]). The motion of a small pellet of the same density as the bulk density of the fluidized particles provided three-dimensional (3-D) information about the particle movement for the first time. An early study of this kind is that of Garncarek et al.,[5] who studied the vertical and horizontal uniformity of occupancy of a pellet tracer in a fluidized bed using PEPT. Also at the Technical University of Delft PEPT was used for studying the particle residence time in interconnected fluidized beds.[6]

Common to all the above investigations is that a pellet of the same density as the bulk density of the bed was used as tracer. Mostoufi and Chaouki[7] investigated the dispersion of a pulse of tracer particles in a fluidized bed by "radioactive particle tracking" (RPT) using normal gamma-ray sources in a single tracer consisting of gold powder and epoxy resin, matching the bed material both in particle density and size. They inferred the

Correspondence concerning this article should be addressed to A. C. Hoffmann at alex.hoffmann@ift.uib.no.

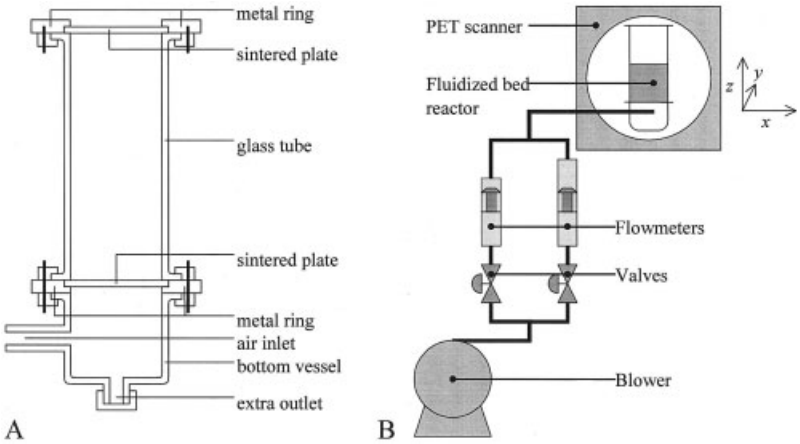


**Figure 1. (A) Fluidized bed vessel; (B) experimental setup and the position of the bed in the PET camera.**

assembly-mean particle behavior from the time-mean behavior of their single tracer particle.

One of the important goals of this present work was to label *actual bed particles* for use as tracer, removing any uncertainties as to whether the tracer acts exactly as the bed particles, and making it possible to study directly the dispersion of *pulses* of particles with time using "positron emission tomography" (PET) rather than PEPT. Using labeled bed particles, the aim was to study

(1) the dispersion of a pulse of particles with time and

(2) the movement of a single particle with high temporal and spatial resolution.

The results for the motion of a single bed particle in a fluidized bed are reported elsewhere.[8,9] The method and equipment used made it possible to draw conclusions about both short-term/small-scale and longer-term/larger-scale particle motion, and the mechanisms causing this motion. That work also showed that the particle position could be determined to within 1 $mm^3$ once every 200 $\mu$s using this method, making the study of processes involving fast particle motion feasible. For the analysis of the fluidized bed it was found optimal in terms of information and computational effort to use only about 1/5 of the data available.

Tracking an individual particle gives information about the nature of fluidized beds and the particle motion in them. If such tracking is done for a sufficiently long time, inferences can, as mentioned, also be made about the time-mean particle motion, which is also the assembly-mean if the process is in steady state.

A more direct way of determining the assembly-mean particle behavior, however, is to study the behavior of *pulses* of marked particles in the bed. The object of the work described in this article was to explore the possibilities and limitations of imaging pulses of radioactive particles in a PET camera for studying particle dynamics in processes involving liquids and/or particles, such as fluidized beds, and to compare the results with a model for the particle dynamics.

## Experimental

### *Setup*

The experimental setup is very similar to the one used for single-particle experiments and is described in detail in Hoffman et al.[8] Only a short description will be given here.

Figure 1 shows the fluidized bed vessel used and a sketch of the rig with the fluidized bed placed in the cylindrical sensing zone of the PET camera. A cylindrical glass column was used as the bed vessel (height 35 cm and diameter 15 cm; these dimensions were chosen to fit the column in the PET scanner sensing zone). Sintered plates were mounted both on the top and on the bottom of the column. The plate at the top prevented the particles from exiting the bed and had a high porosity and a low pressure drop. The plate at the bottom acted as a distributor plate for the gas, and had a lower porosity, formally giving sufficient pressure drop to distribute the fluidizing gas well over the cross section.

Two types of particles were used for the experiments, whose physical properties are shown in Table 1.

The Lewatit MP500 is a macroporous anion-exchange resin, which could easily be labeled with the radioactive tracer. Making use of the anion-exchange mechanism, enough labeler could be attached even to perform experiments with a single particle as a tracer; these experiments are reported elsewhere.[8,9] The FCC catalyst powder was supplied by Shell Global Solutions. It was porous, providing enough surface area to label a pulse of particles. The particle densities given in Table 1 are envelope densities (including the internal pores in the particle volume), not skeletal densities.

Thus for both types of powders the tracer was simply labeled bed particles, making it certain that the behavior of the tracer particles is typical for that of the bulk particles.

The procedure for labeling the particles was as follows: 3 g of particles were soaked in a solution containing 1500 MBq $^{18}F$ in 150 mL demineralized water. After being stirred for 15 min, the material was separated from the water using a Büchner funnel with sintered plate. The marked particles were dried in a small reactor by fluidizing for 0.5–1 h together with 900 mL (in the case of the Lewatit MP500, 1400 mL in the case of the

**Table 1. Physical Properties of the Powders Used**

| | Lewatit MP500 | FCC Catalyst |
|---|---|---|
| Average particle size, $\mu$m | 470 | 79.5 |
| Density, $kg/m^3$ | 1060 | 1464 |
| Sphericity | 1 | 0.9 |
| $\varepsilon_{mf}$ | 0.42 | 0.45 |
| Geldart group | B | A |

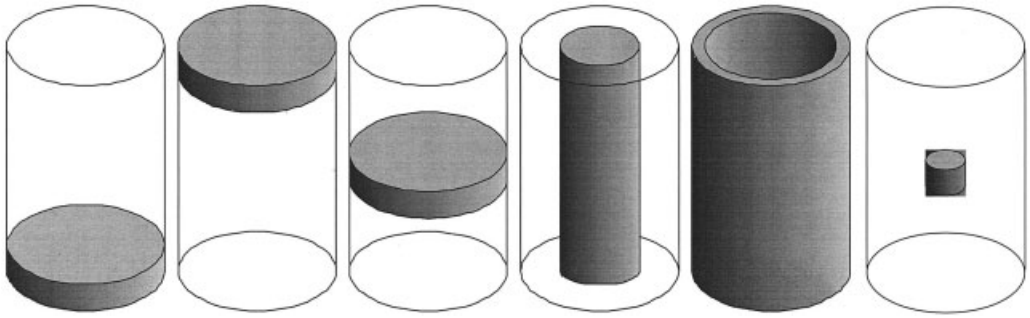

**Figure 2. Types of pulses used in the experiments.**

FCC powder) dry particles. The resulting dry powder constitutes the "tracer." In the case of the FCC catalyst, the initial activity was measured to be about 400 MBq.

The pulse of tracer was arranged in a bed of unmarked particles according to a preplanned scheme (see below), and the bed placed in the PET camera. The camera was started up a couple of seconds before the gas was charged to the bed. The fluidizing gas pump was started up, and initially the gas was discharged to the atmosphere. At $t = 0$, the gas was suddenly diverted to the bed. The fluidization was initiated in this way to minimize startup effects to get as true as possible a picture of the dispersion of the tracer pulse in the bed at steady operating conditions. No atypical behavior of the single-particle tracer just after startup was seen in the single-particle experiments using this procedure.

The height of the powder bed was 20 cm in all cases; for the coarse Lewatit MP500, this remained almost the same when fluidizing at the low excess gas velocities used for these experiments, whereas the bed height rose to about 25 cm when fluidizing the much finer FCC powder. The point in time at which the gas was diverted to the bed could always be recognized by the pulse rising.

### *Plan*

The experiments carried out were based on the following idea: arrange a well-defined pulse of marked particles in the bed, fluidize the bed, and study the dispersion of the pulse through the bed. To minimize startup effects, the flow rate of the fluidizing gas was, as mentioned, set while bypassing the bed, and then suddenly diverted to the bed, so that the proper rate was reached as quickly as possible.

Different types of pulses were used, as illustrated in Figure 2. The three first ones, layers at the bottom, top, and middle of the bed, were intended to show the axial particle dispersion in the bed; the next two, central and annular columns, to show the radial particle dispersion. The last one, a disk in the middle of the column was intended to give and overall impression of the particle mixing in the bed.

The measured superficial velocity required to just fluidize the powder or "minimum fluidization velocity," $U_{mf}$, of the Lewatit MP500 powder was 0.116 m/s, and the experiments were carried out at 0.130 m/s, whereas for the FCC powder the measured $U_{mf}$ was 0.004 m/s, and the experiments were carried out at 0.01 m/s.

## Data Analysis

The camera used was an ECAT EXACT HR+ PET camera. The PET technique is based on the radioactive decay of a radioactive labeler, here $^{18}F$, which leads to the emission of a positron and neutrino. The positron travels a few millimeters through the medium before annihilating with an electron. This annihilation normally results in the emission of two photons, in this case of 511 keV. For energy conservation, the two photons are normally emitted back to back, and thus define a straight line going through the annihilation site.

The emitted photons are detected by cylindrically arranged sensors consisting of 72 blocks, each an array of $8 \times 8$ detectors. In depth there are four such rings of blocks, giving $4 \times 8$ detector rings and $4 \times 72 \times 64$ detectors in total. The dimensions of the detectors are $4.29 \times 4.05$ mm in the angular and $y$-direction, respectively. There is some space between the detectors; the diameter of the detector ring is 83 cm and the depth of the field of view 15 cm.

If two detections are within a narrow time window, they are adjudged to have emanated from the same annihilation, and a "line of response" (LOR) is drawn between them, the position of which is stored as:

- its distance to the camera center
- its angle with the vertical
- the numbers of the two detectors in the direction normal to the paper

We first focus on detections in one particular detector ring (that is, in the $y$-plane). If the angle $q$ was given in radians and the distance $d$ in some unit of length (see Figure 3A), $d$ would be a function of: $r \cos[\theta + \arctan(z/x)]$. Thus, a plot of $d$ vs. $\theta$ would give a sinusoidal shape, the phase and amplitude depending on the position of the point. The range of $\theta$ needs only be from 0 to $\pi$ because of the symmetry of the system.

A *sinogram* (detailed information about the construction of sinograms can be found in Nichols[10]) is a 2-D array containing values of $\theta$ in the rows and values of $d$ in the columns, and is thus equivalent to a plot with $\theta$ on the vertical axis and $d$ on the horizontal one, as the one shown in Figure 3B. In a sinogram, however, both $d$ and $\theta$ are given in terms of *number of detectors*, rather than a length unit and radians, giving a distortion compared to the plot in Figure 3B.

Thus, if the sinogram cells corresponding to the LORs going through one point are marked, a sort of sinusoidal trace, somewhat distorted compared to the traces in Figure 3B, would result. The trace in the sinogram resulting from some pulse of

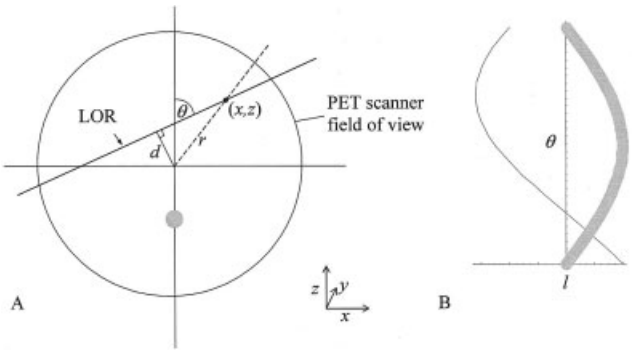


**Figure 3. (A) Sketch of an LOR through a given point (*x*, *z*), and its defining parameters; a circular pulse of radioactive material is also sketched; (B) sketch showing "traces" of the point and the pulse in a plot of *q* vs. *d*.**

Note that the definitions of the coordinate directions differ from the papers dealing with single-particle tracers.[8,9]

active material, such as that indicated in gray in Figure 3A, will result from combining the traces generated by the differential areas making up the pulse. The original spatial shape of any pulse can be reconstructed from the sinogram.

The above explains the organization of the LOR data in one ring, that is, at one particular *y*-position; the *y*-coordinate is given by the number of the ring.

However, the two ends of LORs will also have an impact on detectors in different rings. To make use of these, the detector rings are split in halves, and opposite halves of two rings paired to generate a sinogram. Thus, many sinograms are generated between the possible ring pairs. To limit storage space, the number of sinograms is reduced by grouping them together.

When reconstructing the 3-D image from the sinograms, attenuation of the gamma rays traveling through the medium is corrected for by transmission measurements, measuring the attenuation of gamma rays sent through the subject by the scanner itself.

In our case, transmission measurements were performed with built-in rotating rod sources containing 68Ga/68Ge. During emission measurements the rod sources were retracted in lead shielding inside the PET scanner.

Image reconstruction was done by filtered backprojection. A Hanning filter was used with a cutoff frequency at 0.5 cycles/pixel.

The reconstructed images are stored in so-called image files. In the case of the ECAT EXACT HR+ scanner an image is stored as radiation intensity in 128 × 128 × 63 voxels (3-D pixels of 5.148 × 5.148 × 2.381 mm). For this research, these images were constructed once per second and converted into files of one-byte numbers representing one voxel.

Software was developed in-house,[11] making it possible to analyze the intensity data in the three coordinate planes, as indicated in Figure 4.

The data were suitably averaged and normalized. Figure 5 illustrates how. In Figure 5A data for *y*-planes are tabulated. To eliminate differences in absolute intensity between time frames because of radioactive decay during the experiment, and because of different levels of intensity at $t = 0$ between experiments, all the intensity values were summed at each time frame (A to B in the figure), and normalized to all sum to unity (B to C). To minimize noise, the minimal value for all the time frames was then subtracted from all the values (C to D), and finally the data were again normalized to sum to unity (D to E).

The software has three functions:

(1) Analyzing the raw data as mentioned above and writing the results to ASCII files for further analysis and visualization.

(2) Creating bitmaps giving the intensity distribution in *x*-, *y*-, or *z*-planes.

(3) Tracking a single particle tracer by searching for the voxel with maximal intensity in each time frame for single particle experiments.

As described in Hoffmann et al.[8,9] the last option has been superseded with particle tracking by cross-correlation based on the output in the list-mode files.

Some blurring of the images takes place as a result of the unavoidable scatter in the LORs obtained. Scatter is attributed to a number of effects:

(1) The finite size of the detectors limits spatial resolution, and therefore the LOR precision.

(2) The positron travels a few millimeters through the medium before annihilating with an electron.

(3) The emission of photons may not be exactly collinear; this depends on the momentum of the electron-positron pair before the annihilation.

(4) Gamma rays may be deflected on the way to the sensors by (Compton) scattering.

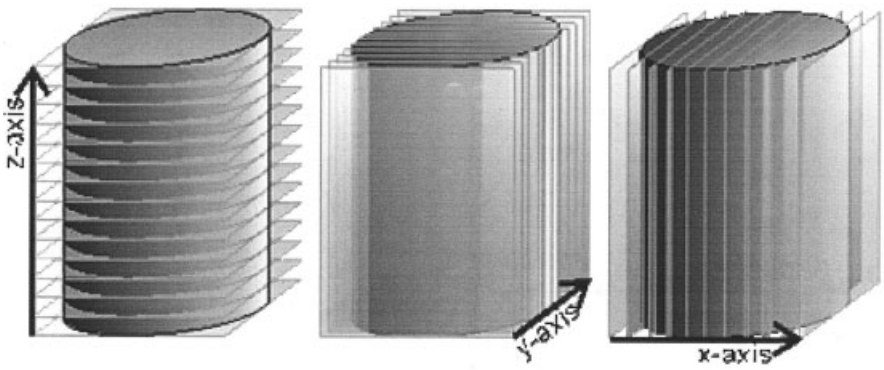


**Figure 4. Analysis of the intensity data from the image files by the in-house software.**

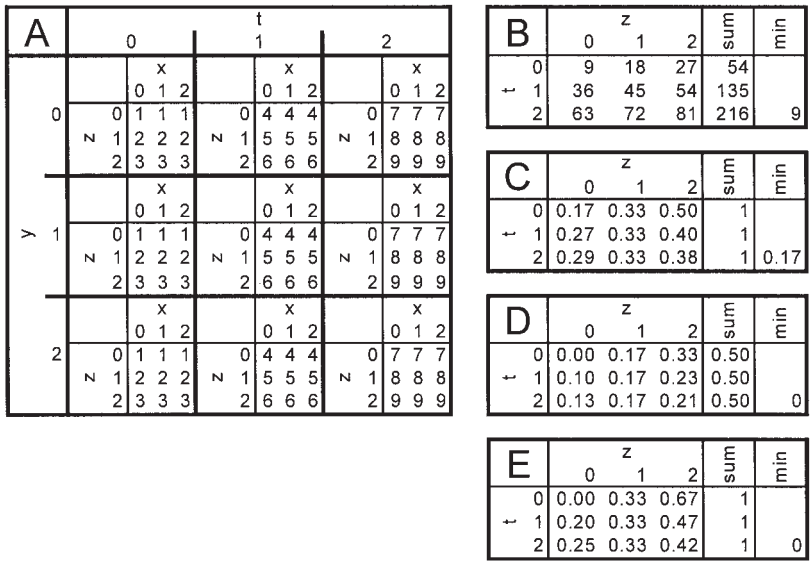


**Figure 5. Illustration of the data treatment.**

Signals from gamma rays that have suffered Compton scattering, and therefore lost some energy, are to some extent suppressed by the electronic setup of the PET scanner, which tags a signal as arising from a gamma ray having suffered scatter if it falls below a preset energy threshold.

Moreover, completely false LORs, which give rise to noise in the images, are obtained as a result of "random coincidences." In random coincidences two different events both give rise to single detections within the same time window, the other photons from both events either penetrating the sensors undetected or falling outside the detection zone, thus giving a poor LOR. Although it is impossible to identify and eliminate the actual false LORs, the *number* of random coincidences, which is roughly proportional to the square of the activity in the sensing zone and therefore limits the total activity that can practically be used, are estimated. This is done using a buffer, which delays a time window. If single signals are detected in both the current window and the delayed window, this is certainly explained by random coincidence. In this way the "noise" arising from random coincidences is estimated and can be subtracted from the signal before image reconstruction.

The intrinsic spatial resolution of the ECAT EXACT HR+ camera is 4–5 mm. The total coincidence count rate, consisting of both true and rejected LORs, may, in the setup used, rise to more than 500 kcps, and did in fact do so during the single-particle experiments. The rejected LORs accounted for about 6% of the total.

## Results and Discussion

The results will be presented as bitmaps showing the marked particle concentration in the bed in a succession of 1-s time frames, and in the form of 3-D plots and contour plots of the marked particle concentration as a function of position in the bed and time.

We start by the axial particle mixing by showing the dispersion of horizontal layers, and then the radial particle mixing by showing centrally and annularly placed particle pulses.

### *Axial particle mixing*

Figure 6 shows the dispersion of a horizontal layer initially placed at the top of a bed consisting of FCC catalyst particles.

The bitmaps and the 3-D plot show the layer first moving upward and then descending through the bed while being dispersed. Once reaching the bottom of the bed, the layer is rapidly brought to the top, where it is still vaguely recognizable, whereafter it again descends and disperses completely.

Figure 7 shows similar results for a layer initially positioned in the middle of the bed. This figure also shows a contour plot for the relative radiation intensity as a function of height and time. Here also, we see the layer initially briefly ascending and then descending while being dispersed. It is then brought quickly to the top of the bed, and descends again while being dispersed further. The 3-D plot shows the descent of the layer as a series of successive ridges with the same slope in the height–time plane. In the contour plot this is visible as light streaks with the same slope in the height–time plane.

The initial ascent of the layer is explained by the fluidizing gas entering the bed and forming fluidization bubbles, expanding the bed, and the layer descent sets in once the fluidization bubbles have reached the layer. Thus the experimental procedure unavoidably leads to a startup effect during which the layer ascends slightly and is not dispersed to any significant extent. The further features can be related to the particle transport associated with the fluidization bubbles, and this will be discussed in the following section, where the results will also be compared with a mathematical model.

The method of Mostoufi and Chaouki[7] of drawing inferences about the dispersion of a pulse from measurements on a single particle based on the principle of ergodicity, gave them quantitative information about dispersion coefficients. However, such a method cannot give information about the organized movement associated with bubble motion, or give the sequen-

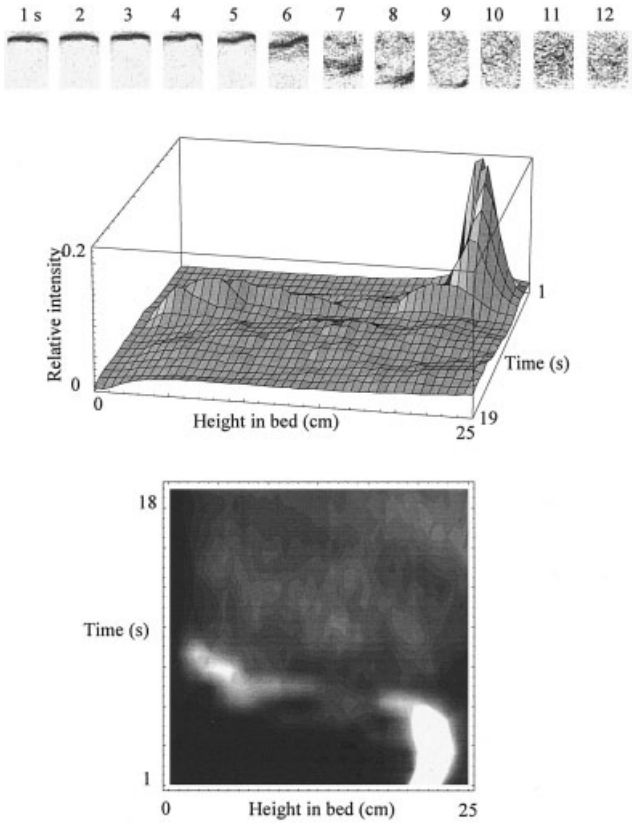


**Figure 6. Dispersion of a horizontal layer from the top of a bed of FCC catalyst powder shown by a series of *x–z* bitmaps, a 3-D plot of *x–y*-averaged tracer concentration (relative radiation intensity) vs. height in the bed and time, and a height–time contour plot of *x–y*-averaged tracer concentration.**

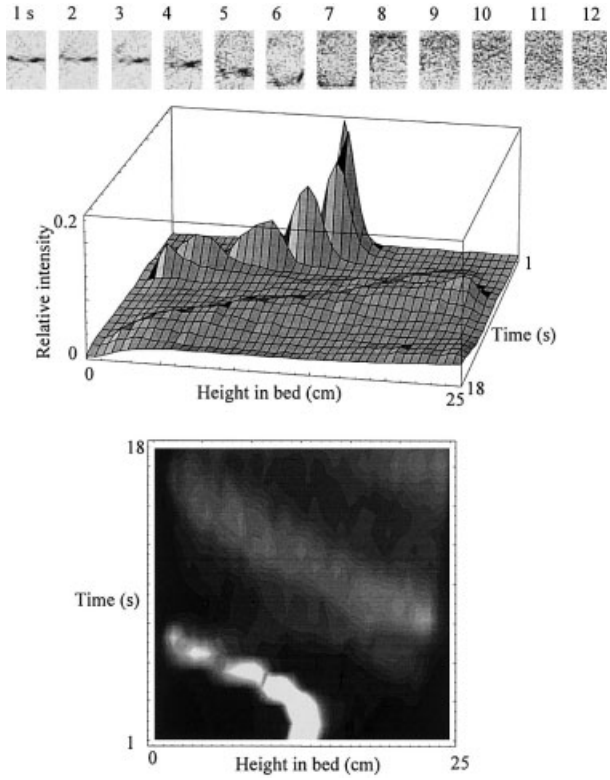


**Figure 7. Dispersion of a horizontal layer from the middle of a bed of FCC catalyst powder shown by a series of *x–z* bitmaps, and a 3-D plot and a height–time contour plot of *x–y*-averaged tracer concentration.**

tial information shown in Figures 6 and 7. Results such as those in Figures 6 and 7, or their matching by a mathematical model as described below, can be achieved only by using the method described here.

For comparison with the results from the FCC powder, the dispersion of a middle layer in a bed of Lewatit MP500 powder is shown in Figure 8. As mentioned, this powder is much coarser than the catalyst powder, and the superficial fluidization velocity in excess of the minimal fluidization velocity, $(U - U_{mf})$, which determines the bubble activity (see below), is much larger. This explains the relatively rapid dispersion of the layer. The values of $(U - U_{mf})$ used were chosen to most clearly show the particle dynamics both through pulse dispersion and single-particle motion.

The dispersion of a layer initially in the bottom of a bed of FCC catalyst is shown in Figure 9.

A degree of asymmetry between the left- and right-hand sides of the bed is evident in all series of bitmaps.

We will discuss these results, their relation to the physical events in the bed, and their comparison to a stochastic model for particle transport in fluidized beds after having shown some results for the radial particle mixing.

### *Radial particle mixing*

Figures 10 and 11 show the radial dispersion through a bed of FCC catalyst particles of pulses initially shaped as a column in the middle and an annular cylinder, respectively.

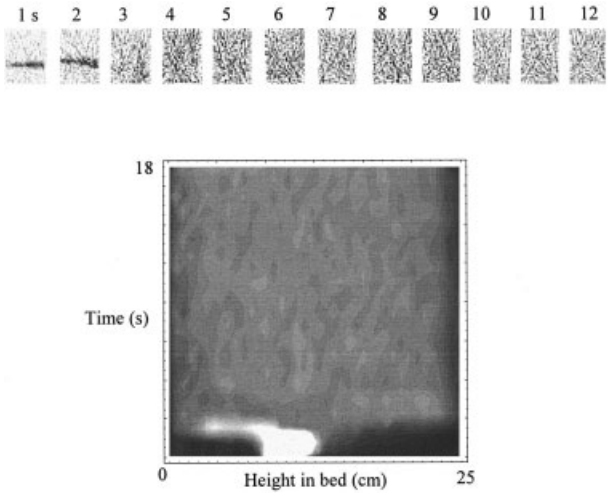


**Figure 8. Dispersion of a horizontal layer from the middle of a bed of Lewatit MP500 shown by a series of *x–z* bitmaps and a height–time contour plot of *x–y*-averaged tracer concentration.**

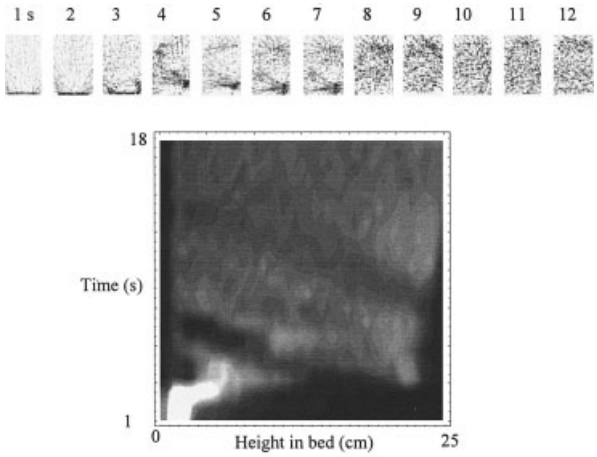


**Figure 9. Dispersion of a horizontal layer from the bottom of a bed of FCC catalyst powder shown by a series of *x–z* bitmaps and a height–time contour plot of *x–y*-averaged tracer concentration.**

A comparison of the two figures makes it clear that the central column remains recognizable for a couple of seconds more than the annular pulse. This, however, was not always the case, and only detailed analysis of the data will show whether the radial dispersion is fastest in the central or the wall region of this bed. It is our general impression that radial dispersion is slower than axial dispersion, consistent with the results of Mostoufi and Chaouki,[7] although our results are somewhat less clear because of the horizontal nonuniformity of the bubble flow.

Figure 12 shows the axial and radial dispersion of the disc-shaped pulse in the middle of the bed. The axial dispersion (left contour plot) shows the same characteristics as the middle layer, with descent and dispersion interrupted by fast movement to the top of the bed, whereas the radial dispersion shows a pattern similar to that of the central column, except that

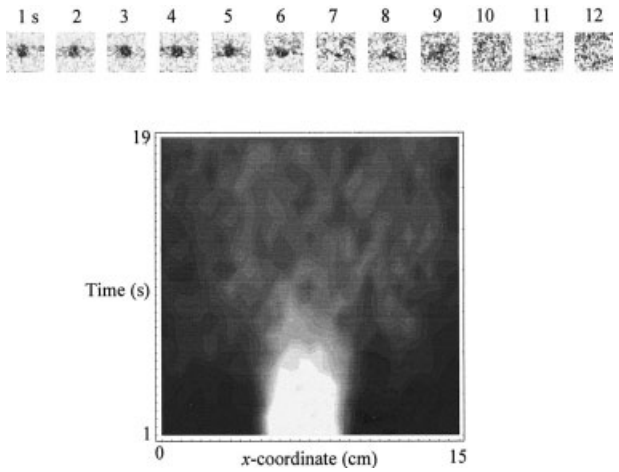


**Figure 10. Radial dispersion of a vertical central column spanning the length of a bed of FCC catalyst powder, shown by a series of *x–y* bitmaps and an *x*-time contour plot of *y–z*-averaged tracer concentration in a central *y*-slice of the bed.**

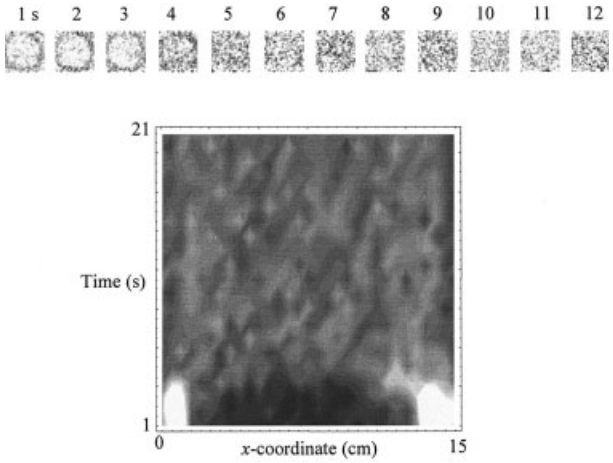


**Figure 11. Radial dispersion of an annular column spanning the length of a bed of FCC catalyst powder shown by a series of *x–y* bitmaps and an *x*-time contour plot of *y–z*-averaged tracer concentration in a central *y*-slice of the bed.**

left–right asymmetry in the *x*-direction is clearer in this case, also consistent with the bitmaps.

## Explanation of the Results and Comparison with a Model

We start with a short description of a phenomenological stochastic model for particle dynamics in a fluidized bed and also mention how the model parameters are obtained. We then compare the model characteristics with the experimental results.

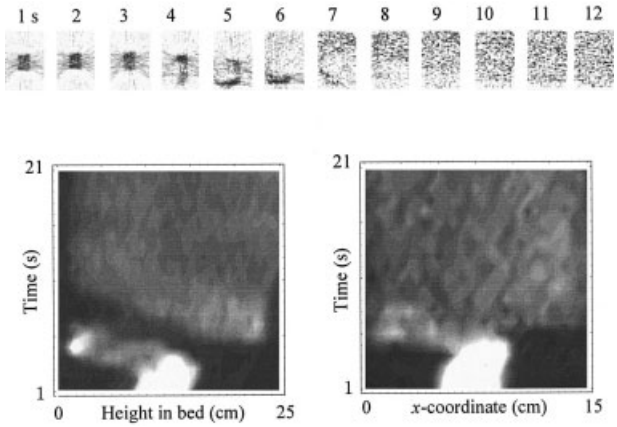


**Figure 12. Axial and radial dispersion of a centrally placed disc in a bed of FCC catalyst powder, shown by a series of *x–z* bitmaps of the concentration of tracer in a central slice (*y*-plane) vs. height in the bed and time, a height–time contour plot of *x–y*-averaged tracer concentration, and an *x*-time contour plot of *y–z*-averaged tracer concentration in a central *y*-slice of the bed.**

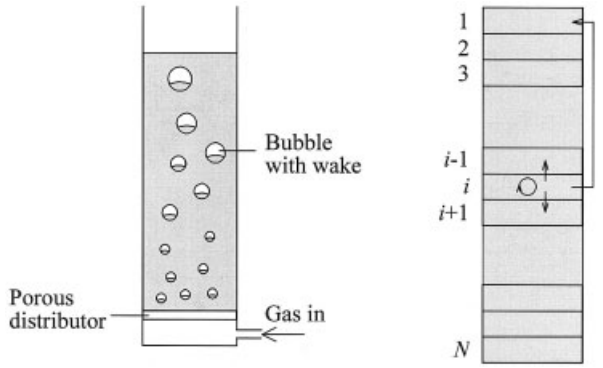


**Figure 13. A batch fluidized bed and a discretized bed.**

### *Particle transport mechanisms and model description*

Rowe and Partridge[12] proposed that the fluidization bubbles are the cause of circulation and dispersion of particles in the bed (see the schematic diagram of a fluidized bed to the left in Figure 13). When bubbles are formed at the distributor plate they collect some particles, forming their so-called *wake*, which moves with the bubble. During the upward motion, wake particles may exchange with bulk particles in the bed until the wake is deposited at or near the surface of the bed. Although the total volume flow of gas in the empty part of the bubbles remains approximately constant axially (see below), the bubbles grow by coalescence. Larger bubbles have an increased wake fraction, so that the material flow in the wake phase increases with height in the bed, and material is taken up in bubble wakes not only at formation at the distributor plate but throughout the bed. For continuity the upward flow in the wake phase causes an equal and opposite downflow in the bulk phase. These two flows together are referred to as "circulation." The bubbles also have the effect of dispersing the bulk particles.

The model used here is based on these concepts and on Dehling and Hoffmann's modeling concepts for particle transport in bubbling fluidized beds based on a convection–diffusion process.[13] In this article we study a batch-fluidized bed, where no inflow or outflow of the particles occurs during the process.

In the model, the motion of one particle is considered, and the transport processes mentioned above are converted to transition probabilities between cells in a discretized bed (see Figure 13). The probability distribution for the particle's position as a function of time reflects the behavior of a radioactive pulse of tracer particles, such as in the experiment. The model is based on Markov chains, such that the transition probability distribution of a single particle is independent of the past history of the system. At the present time, we model only the vertical position of the particle, neglecting the horizontal displacement.

In our discrete Markov model, the reactor is divided into $N$ horizontal cells, and we model the particle's position at discrete times only. The cells are numbered as shown in Figure 13. The model calculates the probability distribution of the axial position of one particle as a function of time. The possible transitions are:

- staying in the same cell
- moving to the next cell
- moving back to the previous cell
- being caught up in a bubble wake and deposited at the top of the bed

We introduce parameters $\alpha_i$, $\beta_i$, and $\delta_i$, with sum equal to 1, for the first three probabilities, conditionally on the particle not being caught up in a bubble wake, the latter probability being given by $\lambda_i$.

The transfer probabilities from cell $i$ to cell $j$ form a matrix, $\mathbf{Q}$, with the elements $q_{i,j}$. The transition probabilities for the interior of the reactor, that is, for $2 \le i \le N - 1$, are

$$q_{i,i} = \alpha_i(1 - \lambda_i) \qquad q_{i,i+1} = \beta_i(1 - \lambda_i) \qquad q_{i,i-1} = \delta_i(1 - \lambda_i) \qquad q_{i,1} = \lambda_i \quad (1)$$

Regarding the boundaries, that is, $i = 1$ and $i = N$,

$$q_{1,1} = 1 - \beta_1(1 - \lambda_1) \qquad q_{1,2} = \beta_1(1 - \lambda_1) \qquad q_{N,N} = 1 - \delta_N(1 - \lambda_N) - \lambda_N$$

and

$$q_{N,1} = \lambda_N \qquad q_{N,N-1} = \delta_N(1 - \lambda_N)$$

The probability distribution of the position of the particle at the $n$th time step is given by the probability vector $\mathbf{p}(n)$, with elements denoted by $p(n, i)$. Knowing $\mathbf{p}(n - 1)$, one can find $\mathbf{p}(n)$ from

$$p(n, j) = \sum_{i=1}^{N} p(n - 1, i)q_{i,j}$$

or in matrix notation: $\mathbf{p}(n) = \mathbf{p}(n - 1)\mathbf{Q}$.

After $n$ time steps, we obtain the formula for the probability distribution of position of the particle at time $n$ in terms of its initial probability distribution

$$p(n) = p(0)\mathbf{Q}^n \qquad (2)$$

in which $p(0)$ is the initial condition of particle distribution in the reactor at time $t = 0$.

The model introduced above is a discrete one, but the transfer probabilities will be related to physical parameters describing the particle transport as continuous processes, following Dehling et al.[13] We call the time step $\varepsilon$ and the cell width $\Delta$. By letting $\varepsilon$ and $\Delta$ go to 0, we obtain a discrete Markov chain approximation to a continuous limit process.

The vertical distance from the top of the bed made dimensionless by dividing by the height of the bed is denoted by $z'$ (that is, $z' = 0$ corresponds to the top and $z' = 1$ to the bottom), and the convective axial velocity attributed to circulation by $v(z')$. The dispersion arising from the disturbance by bubbles is denoted by a dispersion coefficient, $\mathcal{D}(z')$. The probability of returns to the top of the bed is described by the probability rate $\lambda(z')$. The parameters in the transition matrix are defined as follows:

$$\delta_i = \frac{\varepsilon}{2\Delta^2}\mathcal{D}(i\Delta) - \frac{\varepsilon}{2\Delta}v(i\Delta) \qquad \beta_i = \frac{\varepsilon}{2\Delta^2}\mathcal{D}(i\Delta)$$

$$+ \frac{\varepsilon}{2\Delta}v(i\Delta)\alpha_i = 1 - \delta_i - \beta_i \text{ and } \lambda_i = \varepsilon\lambda(i\Delta).$$

Both the axial velocity, arising by circulation of particles, as well as the return rate of particles are functions of the particle flow in the wakes of rising fluidization bubbles. If $Q_W$ denotes the absolute value of the wake flow and $A_{bed}$ the cross-sectional area of the bed, we have: $v(h) = -[Q_W(h)/A_{bed}]$ and $\lambda(h) = (d/dh)[Q_W(h)/A_{bed}]$, where $h = (1 - z')H$ is the height in the bed above the gas distributor plate, with $H$ the total height of the bed, and $v(h)$ is taken as positive in the downward direction. Thus, all that is needed to evaluate the model is $Q_W(h)$ and $\mathcal{D}(h)$.

$Q_W(h)$ can be determined from empirical relations in the literature as described below.

The total volume flow of fluidization gas in the bubble phase $Q_B$ is approximately given by the "two-phase theory"

$$\frac{Q_B}{A_{bed}} = U - U_{mf} \tag{3}$$

and is thus independent of $h$. This relation ignores a slight factual dependency on $h$, and also overestimates the bubble flow for finer powders, such as our FCC catalyst powder. It is possible to account for this but, as will be seen below, this is not warranted in this case because other effects give a much more significant deviation between model and experiment.

The fluidization bubble and its wake together form approximately a sphere, and the fraction of this sphere taken up by wake material is approximately[14]

$$f_W(h) = 0.45[1 - e^{-60D_B(h)}]^{2.75} \tag{4}$$

The material flow in the wake phase is then

$$Q_W(h) = \frac{Q_B f_W(h)}{[1 - f_W(h)]} \tag{5}$$

For evaluating $f_W(h)$ the bubble diameter, $D_B(h)$, which varies with $h$ because of agglomeration, can be found from the empirical relationship of Mori and Wen[15]

$$D_B(h) = D_{B,m} - (D_{B,m} - D_{B,o})\exp\left(-0.3\frac{h}{D_{bed}}\right)$$

with

$$D_{B,o} = \frac{1.38}{g^{0.2}}\left[\frac{1}{1000}(U - U_{mf})\right]^{0.4}$$

$$D_{B,m} = 1.49[D_{bed}^2(U - U_{mf})]^{0.4} \tag{6}$$

A value for the dispersion coefficient $\mathcal{D}(h)$ can be found from a literature study of the vertical particle displacement caused by one rising fluidization bubble[16] and calculating $\mathcal{D}(h)$ as the mean square particle displacement caused by fluidization bubbles per second (this is twice the Fickian diffusion coefficient). Again, as will be seen below, the exact value of $\mathcal{D}(h)$ is not an issue here because other factors cause a large deviation between model and experiment.

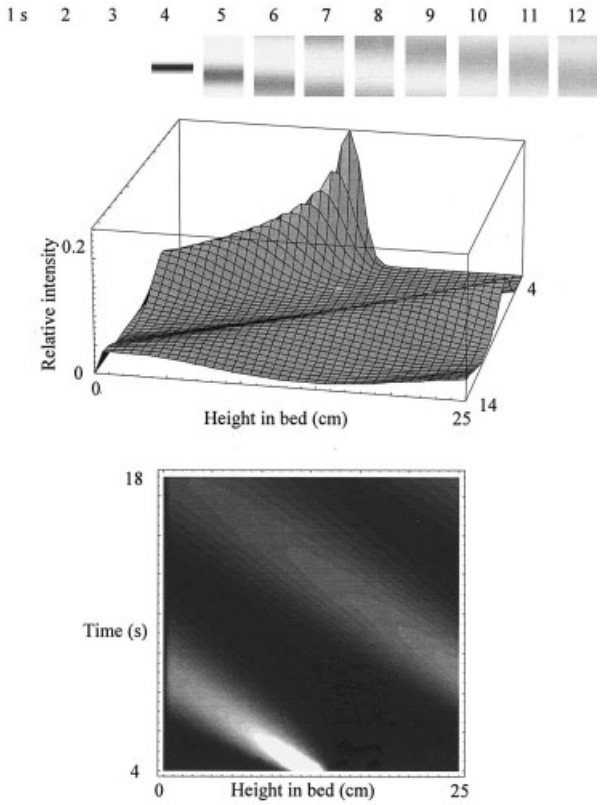


**Figure 14. Model predictions of dispersion of a horizontal layer from the middle of the bed.**

Compare with the experimental results in Figure 7.

### *Comparison between model and experimental results*

When performing a comparison between model and experiment, it must be realized that the model accounts only for the system's behavior after fluidization has been commenced *and* the bubble stream has reached the layer.

Because the bubble flow is low, we can take the superficial downward velocity of the bulk phase to be about $Q_W(h)/A_{bed}$. The above equations then predict bulk descent velocities of about 0.001 m/s, whereas the downward velocity of the pulse in the bulk phase (see for instance Figure 6) seems to be of the order of 0.05 m/s, given that the pulse travels from the top to the bottom of the bed in 4–5 s. We will return to the reason for this discrepancy in the following section. Below we show that upward transport of the particles associated with the bubble flow and downward flow with dispersion in the bulk can qualitatively explain all the features of the experimental results.

Figures 14 and 15 show model output for the dispersion of the middle layer and the top layer, respectively, in the FCC catalyst bed. As indicated by the numbers given above for the expected and actual descent velocity of the layer, the circula-

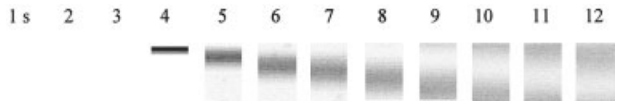


**Figure 15. Model predictions of dispersion of a horizontal layer from the top of the bed.**

Compare with the experimental results in Figure 6.

tion rate $v(h)$, and therefore $Q_W(h)$, had to be multiplied by a factor of 50 to give the fit shown. The dispersion $\mathcal{D}(h)$ had to be multiplied by a factor of 20 for the model to fit the data. The output from the model should be compared with Figures 7 and 6 for the middle layer and the top layer, respectively.

The model predictions clearly account for all the features of the experimental results. More detailed analysis shows that an even better fit to the experimental results could be achieved if not only the descent was associated with dispersion, but also the fast material transport to the top of the bed with the fluidization bubbles was associated with some dispersion. This, of course, is quite reasonable in light of the wide spread in the sizes and velocities of fluidization bubbles and the fact, also shown by the single-particle experiments, that particles at the end of their upward trajectory are deposited not exactly at the bed surface, but somewhat scattered axially over the top region of the bed.

## Further Discussion and Conclusions

We attribute the quantitative discrepancy between experiment and model to "gulf streaming" of the solids in the bed. The principle is illustrated in the sketch in Figure 16. Because of a nonuniform bubble distribution over the bed cross section, regions exist where, in addition to the wake material, bulk material (interstitial between the bubbles) is also dragged up with the bubble stream. This flow of bulk material can be considerably larger than the wake flow, also causing a considerably faster downward bulk flow in the rest of the bed. Merry and Davidson[17] were among the first to discuss such maldistribution of bubble activity and the associated solids movement in fluidized beds, and it has also been discussed by a number of other workers (for example, Werther[18] and Farrokhalaee and Clift[19]). Matsen[20] states that gulf streaming of solids in industrial fluidized beds is unavoidable and that this *constitutes a powerful axial mixing mechanism that is often absent in small, laboratory fluidized beds with good gas distribution*. Werther[18] states that even if the gas distribution is perfect at the distributor plate, regions of high and low bubble activity will still develop; higher in the bed the bubbles will have concentrated in the middle because of coalescence, and this will give rise to gulf-streaming effects.

We have shown elsewhere[9] that in the beds of Lewatit MP500 powder the motion of a single particle indicates that gulf streaming is taking place, even though the beds visually appeared to have a reasonably uniform cross-sectional gas distribution. Upon closer examination of the figures herein, it is clear that gulf streaming is taking place: for instance in the 7th bitmap in Figure 6 and the 4th bitmap in Figure 9 it can be seen that a section of the layer is separated from the main part, and moving upward relative to the main part. The ratio of bubble to column diameter is, according to Eq. 6, about 1/10, so these phenomena are associated with the bubble stream as a whole rather than one bubble.

The phenomenon of gulf streaming in fluidized beds is obviously an important one, which should be included in a model for particle dynamics in fluidized beds. Gulf streaming is mathematically fairly easy to incorporate in a stochastic model for vertical particle transport,[13] although it is not easy to model physically. Going from extremely bad to ideal cross-sectional bubble distribution we might expect:

(1) Very bad bubble distribution gives a very localized region of high bubble activity and velocity, the bulk material flows rapidly upward in this region, and relatively slowly down in the rest of the bed.

(2) Better bubble distribution gives a larger region of lower, but still relatively high, bubble activity; the upward flow of bulk material in this region is larger in terms of volume but smaller in terms of velocity than in a). Downward bulk velocity in the rest of the bed is higher than in a). This is what we see in our experiments.

(3) Ideal bubble distribution, where material is brought upward only in bubble wakes; the downward velocity in the bulk is cross-sectionally uniform and low. This is probably the case in the experiments of Snieders et al.[3]

The transition from state (2) to state (3) is not easy to visualize, or to predict. Moreover, any cross-sectional nonuniformity of fluidization bubble flow is likely to be self-augmenting in that the downward flow of bulk material in regions of low activity probably diverts fluidization bubbles away from that region. Also the bed aspect ratio and the absolute gas flow through the bed in excess of the minimum fluidization velocity are likely to play a role in determining the extent of gulf streaming of the solids.

These experiments show that visual observation of the bed is not enough to determine the extent of gulf streaming, and thus the degree of axial particle mixing in the bed. This issue is further discussed in Wright et al.[21] The degree of axial particle mixing will determine, for instance, the particle residence time in continuous beds and the progress of such processes and fluidized bed granulation and coating. Also the axial heat and mass transfer in fluidized beds, and the degree of particle segregation, depend on the axial particle mixing.

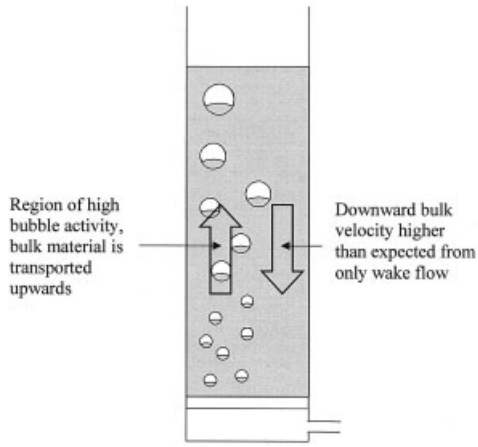


**Figure 16. Illustration of the principle of "gulf streaming" in a fluidized bed.**

Gulf streaming is, as mentioned, likely to be unavoidable in industrial fluidized bed processes. It may in many cases be beneficial in decreasing temperature and concentration gradients in fluidized bed processes. In any case, it is important to model, and to control. Further work is planned to investigate and model gulf streaming in fluidized beds.

## Acknowledgments

The authors are grateful to the following students who provided invaluable help in setting up the experimental system and interpreting the PET camera output: Florence van de Wiel from the University of Groningen and Andrea Ghione from the University of Genova (funded by the SOCRATES program of the EU). They also gratefully acknowledge the cooperation with Dr. Anne Paans and the PET-group at the Academic Hospital in Groningen, The Netherlands, where the experiments were carried out, often after the end of a normal workday. Finally, we are thankful to Dr. Thomas E. Nichols for his assistance in deciphering the data from the camera.

## Notation

$A_{bed}$ = bed vessel cross-sectional area
$D_B$ = diameter of fluidization bubble (twice the radius of curvature of the front)
$D_{B,m}$ = maximal bubble diameter in the bed
$D_{B,o}$ = bubble diameter at the gas distributor
$D_{bed}$ = diameter of the bed vessel
$\mathcal{D}$ = dispersion coefficient (twice the Fickian diffusion coefficient)
$d$ = distance of line of response (LOR) from center of vision
$f_W$ = wake fraction
$g$ = gravitational acceleration
$H$ = height of the bed
$h$ = height in bed, equal to $(1 - z')H$
$i, j$ = indices
$N$ = number of detectors in the ring
$\mathbf{p}(n)$ = probability vector for the particle's position at time step $n$
$p(n, j)$ = elements of $\mathbf{p}(n)$
$Q_B$ = volume flow in the bubble phase
$Q_W$ = volume flow in the wake phase
$\mathbf{Q}$ = matrix of transfer probabilities
$q_{i,j}$ = transfer probability from cell $i$ to cell $j$, elements of $\mathbf{Q}$
$t$ = time
$U$ = superficial gas velocity
$U_{mf}$ = minimum fluidization velocity
$v$ = velocity arising from circulation
$x, y, z$ = Cartesian coordinates, origin in camera center, $z$-coordinate along bed axis
$z'$ = distance from top of bed divided by the total bed height

### *Greek letters*

$\alpha, \beta, \delta, \lambda$ = transfer parameters for a particle in the model
$\lambda(z')$ = probability rate (probability $s^{-1}$) of capture in a bubble wake
$\Delta$ = height of a cell in the discretized bed
$\varepsilon$ = length of a time step
$\varepsilon_{mf}$ = voidage at minimum fluidization conditions
$\theta$ = angle between LOR and the vertical

## Literature Cited

1. Parker DJ, Dijkstra AE, Martin TW, Seville JPK. Positron emission particle tracking studies of spherical particle motion in rotating drums. *Chem Eng Sci*. 1997;52:2011-2022.
2. Stein M, Seville JPK, Parker DJ. Attrition of porous glass particles in a fluidised bed. *Powder Technol*. 1998;100:242-250.
3. Snieders FF, Hoffmann AC, Cheesman D, Yates JG, Stein M, Seville JPK. The dynamics of large particles in a four-compartment interconnected fluidized bed. *Powder Technol*. 1999;101:229-239.
4. Stein M, Ding YL, Seville JPK, Parker DJ. Solids motion in bubbling gas fluidized beds. *Chem Eng Sci*. 2000;55:5291-5300.
5. Garncarek Z, Przybylsk L, Botterill JSM, Broadbent CJ. A quantitative assessment of the effect of distributor type on particle circulation. *Powder Technol*. 1997;91:209-216.
6. Abellon RD, Kolar ZI, den Hollander W, de Goeij JJM, Schouten JC, van den Bleek CM. A single radiotracer particle method for the determination of solids circulation rate in interconnected fluidized beds. *Powder Technol*. 1997;92:53-60.
7. Mostoufi N, Chaouki J. Local solid mixing in gas–solid fluidized beds. *Powder Technol*. 2001;114:23-31.
8. Hoffmann AC, Dechsiri C, van de Wiel F, Dehling HG. PET investigation of the motion of a fluidized particle: Spatial and temporal resolution and short term motion. *Measurement Sci. and Technol.* 2005, in press.
9. Dechsiri, C., Ghione, A. Van de Wiel, F., Dehling, HG, Paans, AMJ, Hoffmann, AC. Positron emission tomography applied to fluidization engineering. *Can. J. Chem. Eng*. 2005, in press.
10. Nichols TE. *Spatiotemporal Modeling of Positron Emission Tomography*. PhD Thesis. Pittsburgh, PA: Dept. of Statistics, Carnegie Mellon University; 2001.
11. van der Zwan EA. *PET: A New Method for Analyzing Fluidized Beds*. MS Thesis. Groningen, The Netherlands: Dept. of Chemical Engineering, University of Groningen; 2001.
12. Rowe PN, Partridge BA. Particle movement caused by bubbles in a fluidised bed. *Interaction Between Fluids and Particles*. London: Institution of Chemical Engineers; 1972:135-142.
13. Dehling HG, Hoffmann AC, Stuut HW. Stochastic models for transport in a fluidized bed. *SIAM J Appl Math*. 1999;60:337-358.
14. Bosma JC, Hoffmann AC. On the capacity of continuous powder classification in a gas fluidized bed with horizontal baffles. *Powder Technol*. 2003;134:1-15.
15. Mori S, Wen CY. Estimation of bubble diameter in gaseous fluidized-beds. *AIChE J*. 1975;21:109-115.
16. Tanimoto H, Chiba S, Chiba T, Kobayashi H. Jetsam descent induced by a single bubble passage in three-dimensional gas-fluidized beds. *J Chem Eng Jpn*. 1981;14:273-276.
17. Merry JMD, Davidson JF. Gulf-stream circulation in shallow fluidized-beds. *Trans IChemE*. 1973;51:361-368.
18. Werther J. In: Keairns DL, ed. *Fluidization Technology*. Washington, DC: Hemisphere; 1975.
19. Farrokhalaee T, Clift R. In: Grace JR, Matsen JM, eds. *Fluidization*. New York, NY: Plenum Press; 1980.
20. Matsen JM. Scale-up of fluidized bed processes: Principles and practice. *Powder Technol*. 1996;88:237-244.
21. Wright PC, Makkawi YT, Meeyoo V, Dechsiri C, van der Zwan E, Paans AMJ, Hoffmann AC. Observation of cross-sectional non-uniformity in fluidized beds using two different imaging techniques. *Proc. of WCPT4, the Fourth World Congress on Particle Technology*, Sydney, Australia; 2002.

*Manuscript received Nov. 18, 2003, and revision received July 7, 2004.*